SCIENCE CHINA
Technological Sciences

•Article•

August 2018 Vol.61 No.8: 1228–1237
https://doi.org/10.1007/s11431-017-9190-2

Mg-Zn-Y-Nd coated with citric acid and dopamine by layer-by-layer self-assembly to improve surface biocompatibility

CHEN Li[1], LI JingAn[1*], CHANG JiaWei[2], JIN ShiBo[2], WU Di[2], YAN HaoHao[2], WANG XiaoFeng[3] & GUAN ShaoKang[1*]

[1] *School of Materials Science and Engineering, Zhengzhou University, Zhengzhou 450001, China;*
[2] *School of Life Science, Zhengzhou University, Zhengzhou 450001, China;*
[3] *National Center for International Research of Micro-nano Molding Technology & Key Laboratory for Micro Molding Technology of Henan Province, Zhengzhou 450001, China*

Received November 8, 2017; accepted January 3, 2018; published online February 2, 2018

Magnesium alloy has been generally accepted as an important biodegradable material on cardiovascular stent development for a long time. However, its limited biocompatibility, especially delayed endothelialization process restricts its further application. In this contribution, we modified the Mg-Zn-Y-Nd alloy surface with citric acid and dopamine via a layer-by-layer self-assembly assay, aiming at improving the biocompatibility of the magnesium alloy. The citric acid/dopamine (CA/PDA) layer exhibited a remarkable suppression of platelet activation/aggregation and thrombosis under 15 dyn/cm^2 blood flowing. Inhibition on vascular smooth muscle cells growth and macrophages attachment/activation were also observed on this layer. In particular, the CA/PDA layer presented a promoted property for the vascular endothelial cells growth and spreading compared with the bare magnesium alloy, suggesting the pro-endotelialized function. In conclusion, this research may support potential application on surface modification of magnesium alloy based cardiovascular stents for better biocompatibility.

cardiovascular stent, Mg-Zn-Y-Nd alloy, biocompatibility, layer-by-layer self-assembly, citric acid, dopamine

Citation: Chen L, Li J A, Chang J W, et al. Mg-Zn-Y-Nd coated with citric acid and dopamine by layer-by-layer self-assembly to improve surface biocompatibility. Sci China Tech Sci, 2018, 61: 1228–1237, https://doi.org/10.1007/s11431-017-9190-2

1 Introduction

According to global non communicable diseases status report 2014 by World Health Organization (WHO), cardiovascular disease (CVD) is still the leading cause of morbidity and mortality globally (there are 17 million thousand deaths because of CVD worldwide each year, far above the 8 million thousand deaths from cancer) [1]. Interventional therapy of CVDs with cardiovascular stents is emerged as the most effective methods in clinical [2]. However, traditional stents (stainless steel stent or cobalt chromium alloy stent, etc.) may stimulate the organisms serious inflammations after implantation for long terms, and further lead to series of complication, which limit the stents long-term application [3,4]. Thus, it becomes a hot research topic that developing biodegradable stents to treat the early vascular occlusion and further promote tissue regeneration during the stents degradation for solving complications of foreign graft implantation [5,6]. Magnesium alloy has been studied a lot as an important biodegradable material on cardiovascular stent development for its excellent mechanical properties and biodegradability [7,8]. In particular, the Mg-Zn-Y-Nd alloy has been reported widely for series superior performance, including better mechanical properties, slower degradation rate, and lower biological toxicity, etc. [9–11]. However, the biocompatibility of the Mg-Zn-Y-Nd alloy still needs to be

*Corresponding authors (email: lijingan@zzu.edu.cn; skguan@zzu.edu.cn)

further improved to satisfy the cardiovascular stent's requirement, such as anti-inflammation, anti-coagulation, anti-hyperplasia and especially pro-endothelialization.

Surface modification is an effective technology to enhance the stents materials' biocompatibility, and the technology includes layer-by-layer self-assembly [12], co-immobilization [13], plasma ion implantation [14], atomizing spraying [15] and polymer deposition [16], etc. For magnesium alloy modification, surface uniform passivation and functional molecular grafting via layer-by-layer self-assembly is the preferable method to enhance its biocompatibility [17,18]. Citric acid solution is a common passivation reagent which has been widely applied for surface modification of magnesium alloy, its application may prevent the alloy substrate from corrosion. Citric acid also exists in human body and involves in the "three carboxylic acid cycle" and "tricarboxylic acid cycle", contributing to the decomposition of fat [19,20]. Its sodium salt has been used in clinical as anticoagulant and anti-inflammation drugs [21]. Dopamine is well known for mussel inspired functions, i.e. its outstanding conjugation for metals and other molecules [22,23]. Polydopamine (PDA) film also possesses friendly property for vascular endothelial cells adhesion and proliferation, which is conductive to the cardiovascular implanted materials' surface endothelialization [24]. Thus, surface modification with citric acid and dopamine by layer-by-layer self-assembly to improve magnesium alloy biocompatibility may be an ideal strategy for biodegradable cardiovascular stent development.

In this contribution, we modified the Mg-Zn-Y-Nd surface with citric acid and dopamine by layer-by-layer self-assembly, and the modified layers were labeled as CA/PDA. The surface morphology and roughness of the CA/PDA layers were characterized by atomic force microscopy (AFM), and their wettability was detected by water contact angle measurement. A dynamic blood experiment was performed to evaluate the blood compatibility, and series of cell experiments were performed to investigate the CA/PDA layers' cytocompatibility.

2 Materials and methods

2.1 Preparation of CA/PDA coating on Mg-Zn-Y-Nd

The Mg-Zn-Y-Nd alloy were cut into small discs with the 10 mm diameter and 3 mm thick, and then polished with metallographic abrasive paper of 100#, 200#, 400#, 600#, 800#, 1000#, successively. Then the Mg-Zn-Y-Nd disks were sonicated successively in acetone, ethanol, and deionized water (dH_2O) and finally dried at room temperature. The clear Mg-Zn-Y-Nd were treated by a citric acid (CA) solution (1 mg/mL) for 1 h, then rinsed with dH_2O for 3 times (5 min per time) to remove the unconjugated CA. After a drying step, the samples were immersed into 2 mg/mL dopamine (PDA) solution (dissolved in pH 8.5 Tris buffer). After deposition for 1 h, the samples were washed in dH_2O, and labeled as CA/PDA-1. After that, 1 mg/mL of CA was in advance activated in water-soluble carbodiimide (WSC) solution composed of 1 mg/mL *N*-(3-dimethylaminopropyl)-*N*′-ethylcarbodiimide (EDC, purity ≥98.0%, Sigma-Aldrich, USA) and 0.24 mg/mL nhydroxysuccinimide (NHS, purity ≥97.0%, Sigma-Aldrich, USA) for 15 min. Then, the CA/PDA-1 were immersed into the above CA solution for incubation. After reaction for 1 h, the specimens were washed with dH_2O (3 times, 5 min) and followed with a PDA deposition as described above, and the samples were labeled as CA/PDA-2. Then, the CA/PDA-2 were treated with CA and PDA via self-assembly again, and were labeled as CA/PDA-3. The pure CA or PDA treated Mg-Zn-Y-Nd for 1 h were used as control, and were labeled as CA and PDA, respectively. The preparation process of the CA/PDA coatings was displayed in Figure 1.

2.2 Surface characterization of CA/PDA coating

The morphologies and roughness of CA/PDA-1, CA/PDA-2, CA/PDA-3, CA, PDA and Mg-Zn-Y-Nd samples were observed by atomic force microscopy (Key sight 7500, USA) in tapping mode and scanning electron microscopy (SEM, JSM-7001F, Japan) [25]. The wettability of CA/PDA-1, CA/PDA-2, CA/PDA-3, CA, PDA and Mg-Zn-Y-Nd sample surfaces was assessed by water contact angle measurement (DSA 100, Krüss, GmbH, Germany) at room temperature followed by image processing of sessile drop of 5 μL test ultrapure water with DSA 1.8 Software. At least 6 contact angles on different areas were measured and averaged [26]. The carboxyl group quantification of HA bound to the surface of coatings was performed by a Toluidine blue-O (TBO) method [27]. The density of amine groups on the PDA/HD coating was determined using Acid Orange II (AO II) colorimetric method [28]. Electrochemical tests were carried out using a classical three electrodes cell with a platinum rod as the auxiliary electrode, a saturated calomel electrode as the reference electrode and the samples as the working electrode. The simulated body fluid (SBF) was prepared according to previous studies [29]. The electrolyte was buffered at pH 7.4 using tris-hydroxymethyl aminomethane ($(HOCH_2)_3CNH_2$) and hydrochloric acid (HCl), kept at 37 °C. The sample area exposed to the solution was 1 cm^2. The measurements were carried out at a scan rate of 0.5 mV/s using an electrochemical station and the sample was kept in the solution for 1 h before polarization tests to establish the open circuit potential [30].

2.3 Dynamic blood test

A dynamic blood test on each sample was performed via

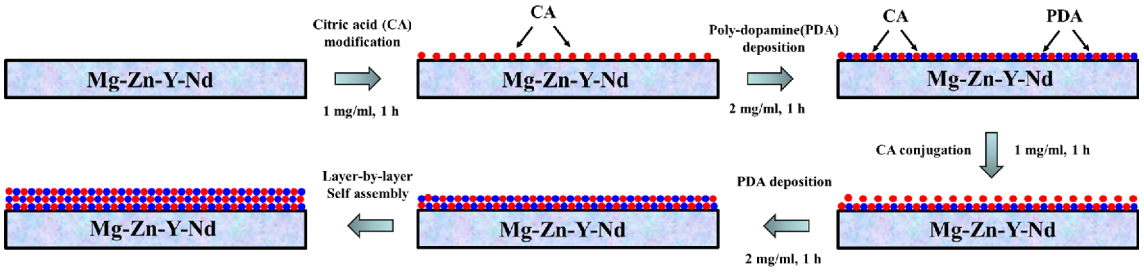

Figure 1 (Color online) The scheme of preparing CA/PDA coatings on the Mg-Zn-Y-Nd surface.

setting them into the 24-well culture plate and being cultured on the shaking table *in vitro* at 37 °C for 1 h. Then, the samples were picked out, washed with PBS (pH 7.4, 3 times, 5 min), and fixed with 2.5% glutaraldehyde solution, dehydrated at increasing alcohol concentrations (50%, 75%, 90%, 100%; $V_{alcohol}$ / V_{dH_2O}) and dealcoholized at increasing isoamylacetate (50%, 75%, 90%, 100%; $V_{isoamyl\ acetate}/V_{alcohol}$), all the samples were dried with critical point drying (CPD030, Balzers, Switzerland) and coated with gold to conduct SEM to evaluate the morphology. The amounts of the adherent platelets and the activated platelets were also detected by the previous method, respectively [31,32].

2.4 Endothelial cells culture

Human umbilical vein endothelial cells (HUVEC) obtained from the newborn umbilical cord (Haoyi Biotechnology Co., Ltd., Chengdu, China) were cultured in a humidified incubator with 95% air and 5% CO_2. HUVEC between 3rd and 5th passages were used for experiments. The CA/PDA-1, CA/PDA-2, CA/PDA-3, CA, PDA and Mg-Zn-Y-Nd samples were placed in a 24-well culture plate, and the HUVEC were seeded onto the samples with the concentration of 5×10^4 cells/mL, then cultured at 37 °C for 1 d. After the sequentially washed step, the samples were fixed with 4% paraformaldehyde (Sigma, USA) for 2 h at room temperature and stained by rhodamine reagent (Sigma, USA) for 15 min, finally examined and recorded by a fluorescence microscope (DMRX, Leica, Germany) [33]. The HUVEC numbers on each sample was detected via a typical CCK-8 method [34].

2.5 Smooth muscle cells culture

Human umbilical arterial smooth muscle cells (HUASMC) were also purchased from Haoyi Biotechnology Co., Ltd. (Chengdu, China), and cultured in a standard condition elaborated above. HUASMC between 2nd and 7th passages were seeded on the CA/PDA-1, CA/PDA-2, CA/PDA-3, CA, PDA and Mg-Zn-Y-Nd samples with the concentration of 5×10^4 cells/mL, and cultured at 37 °C for 1 d. The HUASMC was observed under the fluorescence microscope after the fixed step and stained with 4,6-diamino-2-phenyl indole (DAPI) [35]. The HUASMC number was also examined [36].

2.6 Macrophages attachment

The peritoneal macrophages of SD rats (Haoyi Biotechnology Co., Ltd., Chengdu, China) were also cultured in the standard culture condition, and then added onto each samples with the concentration of 5×10^4 cells/mL, and incubated at 37 °C for 24 h. To study the cell behaviors, the fluorescence staining of the attached macrophages was performed using DAPI, and the numbers of the cells on each samples were statistically counted from 15 random pictures [37].

2.7 Statistical analysis

Mean values±SD are given with their representative images. Statistical significance requires a p-value <0.05.

3 Results and discussion

3.1 Surface characterization

Figure 2 showed the surface roughness changes on the CA/PDA-1, CA/PDA-2, CA/PDA-3, CA, PDA and Mg-Zn-Y-Nd samples. The Mg-Zn-Y-Nd substrate showed an obvious smoother surface with lower roughness (24.7±3.6 nm) because of the polished process, the roughness increased to a very high value (97.3±6.9 nm) after the CA treated for 1 h. Pure PDA preparation markedly showed a smoother surface (59.3±9.1 nm) compared with the pure CA surface, but still showed rougher surface compared with Mg-Zn-Y-Nd substrate. However, the CA/PDA coatings exhibited smoother surfaces compared with both pure PDA and pure CA surfaces, and more self-assembly layers were prepared, smoother the surface developed, indicating a trend of roughness: CA/PDA-1>CA/PDA-2>CA/PDA-3. This phenomenon may be attributed to the property of the self-assembly method, which may make the immobilized molecules showing a more homogeneous distribution, and further the homogeneously distributed PDA makes the surface smoother.

Figure 3 showed the surface morphology on the CA/PDA-

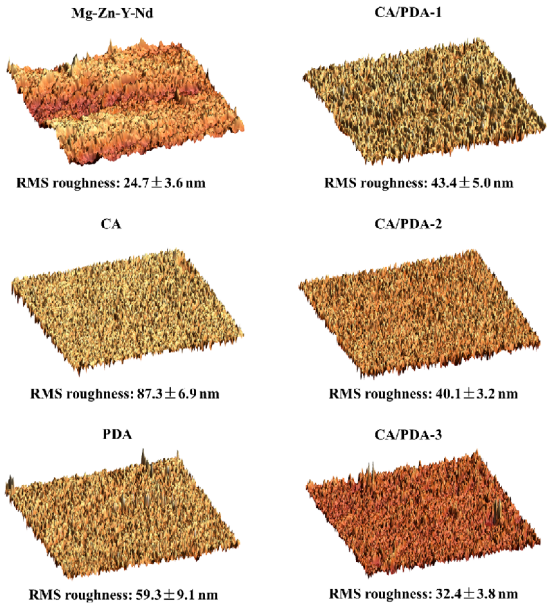

Figure 2 (Color online) AFM images of Mg-Zn-Y-Nd, CA, PDA, CA/PDA-1, CA/PDA-2 and CA/PDA-3 samples (mean±SD).

1, CA/PDA-2, CA/PDA-3, CA, PDA and Mg-Zn-Y-Nd samples. The Mg-Zn-Y-Nd substrate presented a relatively smooth surface, while the lighter stripes and white dots were produced during the polished process, and it was ineluctable. The CA modification covered the stripes, but part of the magnesium alloy substrate was exposed, and this may be due to the inhomogeneous layer prepared by the single modification. All the CA/PDA coatings and the single PDA surface showed several cracks caused by the drying process, and the crack number and width can also indirectly verify the stability of the coatings. Obviously, there were less cracks on the CA/PDA-1 coating compared to the PDA, CA/PDA-2 and CA/PDA-3 surfaces, and simultaneously the cracks on the CA/PDA-1 coating showed narrower width compared with the cracks on the PDA, CA/PDA-2 and CA/PDA-3 surfaces, suggesting better stability of the CA/PDA-1 coating.

Surface hydrophilicity is a factor that influences the biocompatibility of the biomaterials by making quantitative and qualitative variation of the adsorbed protein [38]. In this work, the water contact angles were detected to evaluate the surface hydrophilicity of CA/PDA coatings. Figure 4 showed the water contact angle of the CA/PDA-1, CA/PDA-2, CA/PDA-3, CA, PDA and Mg-Zn-Y-Nd samples. It is clear that Mg-Zn-Y-Nd presented a very high water contact angle (114.4°±5.8°), indicating a hydrophobic surface, and the CA treatment reduced the water contact angle (102.3°±3.0°), but still showed a hydrophobic surface, while PDA deposition significantly made the water contact angles decrease to a hydrophilic range (80.3°±0.7°), indicating a hydrophilic surface. However, the CA/PDA coatings showed a broad range on water contact angles, the increased layers made the values decrease successively: CA/PDA-1 (102.1°±5.9°)>CA/PDA-2 (89°±0.0°)>CA/PDA-3 (61.7°±8.0°).

Quantitative determination of carboxyl and amine groups not only makes positive correlation to the immobilized citric acid and dopamine respectively, but also reveals the trends in biocompatibility on the surface indirectly [39]. Figure 5(a) showed that there was no significant difference between CA and CA/PDA-1 on the carboxyl group density, which indicated that one layer dopamine deposition made minimal influence on the free carboxyl group or citric acid distribu-

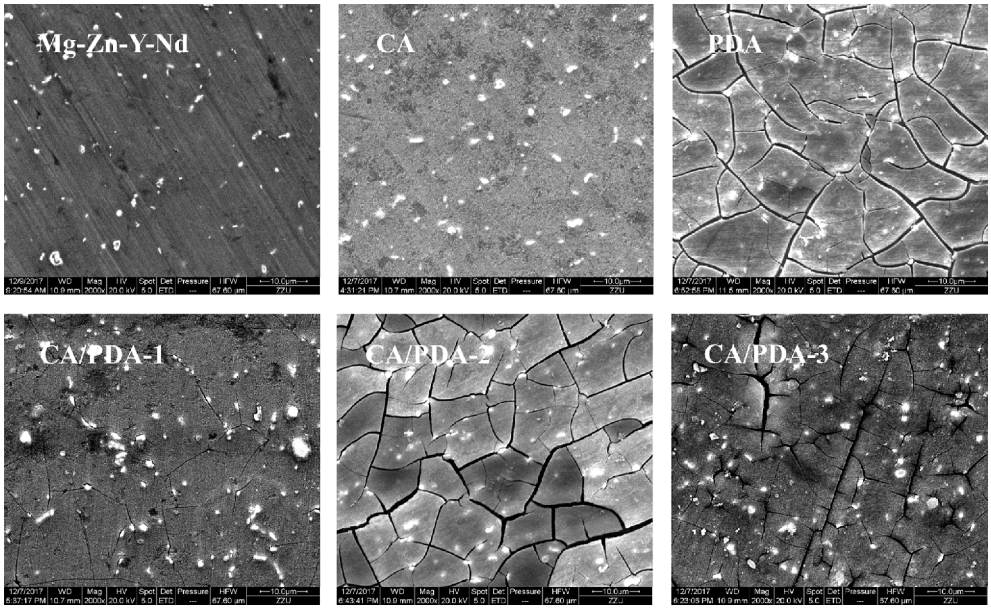

Figure 3 SEM images of Mg-Zn-Y-Nd, CA, PDA, CA/PDA-1, CA/PDA-2 and CA/PDA-3 samples.

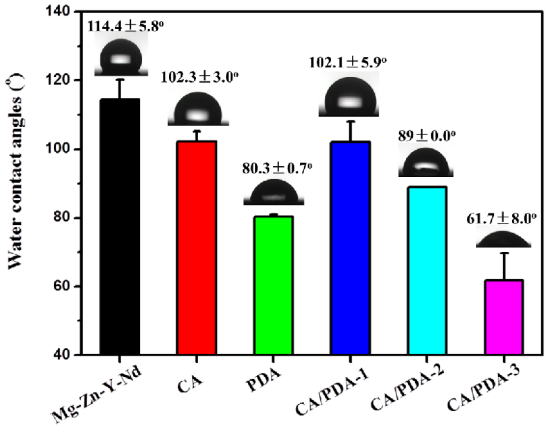

Figure 4 (Color online) Water contact angles of Mg-Zn-Y-Nd, CA, PDA, CA/PDA-1, CA/PDA-2 and CA/PDA-3 samples (mean±SD, n=6).

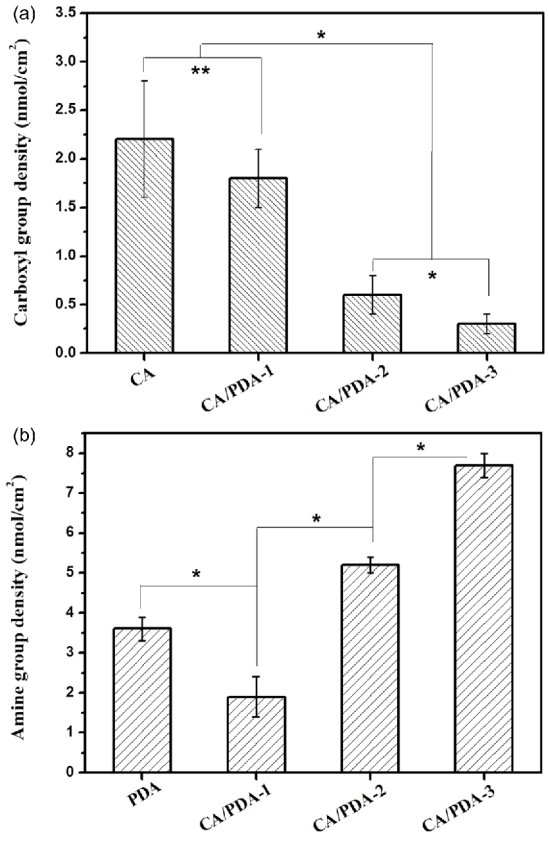

Figure 5 Surface (a) carboxyl and (b) amine group density of each sample (*p<0.05, **p>0.05, mean±SD, n=6).

tion. However, the CA/PDA-2 and CA/PDA-3 surfaces presented a decreasing carboxyl group density compared with CA and CA/PDA-1, suggesting that the more layers structures covered up the free carboxyl groups below. In addition, the interaction between citric acid and dopamine also consumed part of the free carboxyl group. Figure 5(b) showed that the amine groups of CA/PDA-1 significantly decreased compared to PDA, which may be due to the different amounts of the deposited dopamine, because the modified CA possessed part of the Mg-Zn-Y-Nd surface, and this may reduce the amount of the deposited dopamine and also the amine density. The CA/PDA-2 and CA/PDA-3 surfaces presented an increasing amine group density compared with carboxyl group which indicated more free amine group was enriched on the surfaces. The prepared modified layers may regulate the surface biocompatibility by appropriate carboxyl and amine group density [40].

Electrochemical test is a typical method to evaluate the samples' corrosion resistance [30]. Figure 6 presented the typical polarization curves of the CA/PDA-1, CA/PDA-2, CA/PDA-3, CA, PDA and Mg-Zn-Y-Nd samples in SBF. Corrosion potential (E_{corr}) and corrosion current density (I_{corr}) were summarized in Table 1. The previous research indicated that the samples' corrosion resistance was determined by their corrosion current density and resistance [30]. From Figure 6 and Table 1, CA/PDA-1 coating obviously improved the corrosion resistance of the Mg-Zn-Y-Nd substrate, with the corrosion current density decreases from 1.30×10^{-4} A/cm^2 to 4.38×10^{-5} A/cm^2, also suggesting better stability of CA/PDA-1 samples.

3.2 Blood compatibility

The blood flow contacts materials surface that may trigger the adhesion and activation of platelets, thrombosis formation and red blood cells (RBC) adhesion, all of which may lead to restenosis [41]. Therefore, the *in vitro* dynamic blood

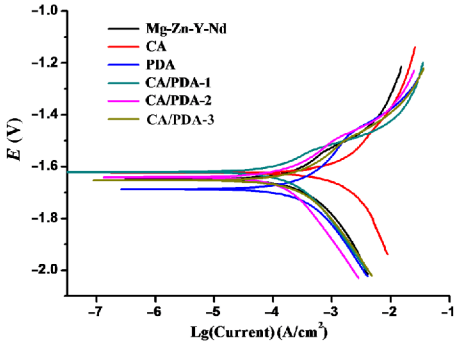

Figure 6 (Color online) Polarization curves of the CA/PDA-1, CA/PDA-2, CA/PDA-3, CA, PDA and Mg-Zn-Y-Nd samples in SBF.

Table 1 Values from the polarization curve of different samples in SBF

Samples	E_{corr} (V)	I_{corr} (A/cm^2)
Mg-Zn-Y-Nd	−1.65	1.30×10^{-4}
CA	−1.62	9.55×10^{-4}
PDA	−1.69	2.32×10^{-4}
CA/PDA-1	−1.62	4.38×10^{-5}
CA/PDA-2	−1.64	1.32×10^{-4}
CA/PDA-3	−1.65	2.00×10^{-4}

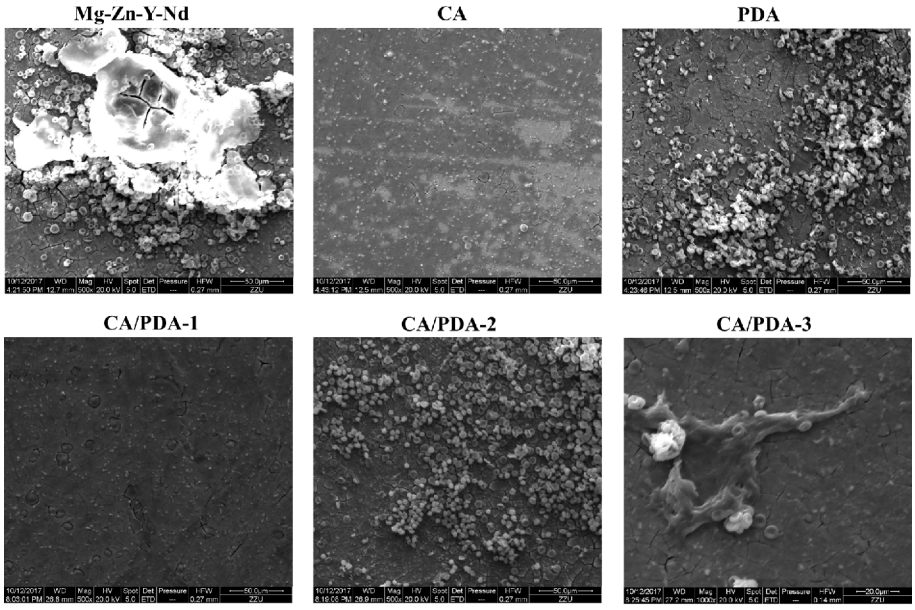

Figure 7 SEM images of adherent blood components (platelets, red blood cells and thrombus) on the CA/PDA-1, CA/PDA-2, CA/PDA-3, CA, PDA and Mg-Zn-Y-Nd samples.

test is often applied to evaluate the blood compatibility of the stents materials surface. SEM images of the adherent blood components on each sample were presented in Figure 7, and this result showed that there were less platelets adherent, thrombosis and RBC on the CA and CA/PDA-1 surfaces compared on the other surfaces. On the Mg-Zn-Y-Nd surface, the adherent platelets/RBC from the blood flow and the corrosion products from the materials stirred together. The PDA surface markedly slowed down the materials corrosion, but more platelets and RBC adhesion and aggregated on its surface due to the amine group. The CA/PDA-2 surface presented more platelets/RBC adhesion/aggregation because of higher amine group density. However, the CA/PDA-3 surface exhibited less adherent platelets/RBC with higher amine group density, and this may be just attributed to its excessive amine group which will lead to suppression on the cells adhesion that was described in the previous work [28], while the obvious thrombosis also indicated a poor blood compatibility. The quantitative characterization of adherent/activated platelets by the typical LDH/GMP140 methods presented the consistent results: CA and CA/PDA-1<CA/PDA-3<Mg-Zn-Y-Nd<PDA<CA/PDA-2 (Figure 8), which indicated better blood compatibility of CA and CA/PDA-1 surfaces.

3.3 Vascular endothelial cells growth

To investigate the endothelial cells growth on CA/PDA-1, CA/PDA-2, CA/PDA-3, CA, PDA and Mg-Zn-Y-Nd, HUVEC were seeded on the surface of each sample. After culture for 1 d, the morphology and behavior of HUVEC were observed by fluorescence images in Figure 9. The HUVEC

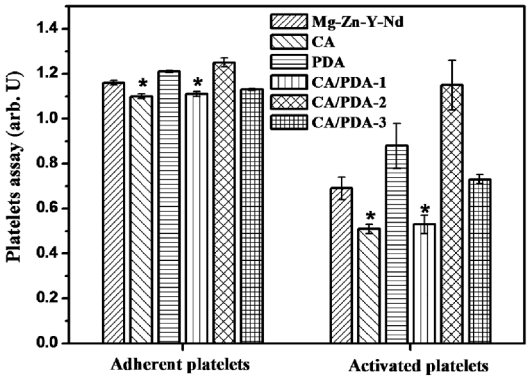

Figure 8 Quantitative characterization of adherent (LDH) and activated (GMP140) platelets on the CA/PDA-1, CA/PDA-2, CA/PDA-3, CA, PDA and Mg-Zn-Y-Nd samples (mean±SD, *p<0.05 compared with other samples, n=3).

on Mg-Zn-Y-Nd presented shrunken or dilapidated morphology as description by the research elsewhere [42], and the CA modification further aggravated this phenomenon due to the rich carboxyl group. The PDA modification increased the surface HUVEC number and coverage ratio by introducing amine group. The CA/PDA-1 further improved Mg-Zn-Y-Nd surface endothelialization by strengthening its corrosion resistance function and controlling the amine density to an appropriate value. The increased amine density but decreased HUVEC number on the CA/PDA-2 and CA/PDA-3 surface was evidence that surface amine density distributed in appropriate range really affect cells growth. Combining with the RBC numbers in Figure 7, there was obviously distinct response from different cells (HUVEC and RBC, etc.) for the amine density change. The HUVEC on CA/PDA-2 and CA/PDA-3 surfaces also showed lower

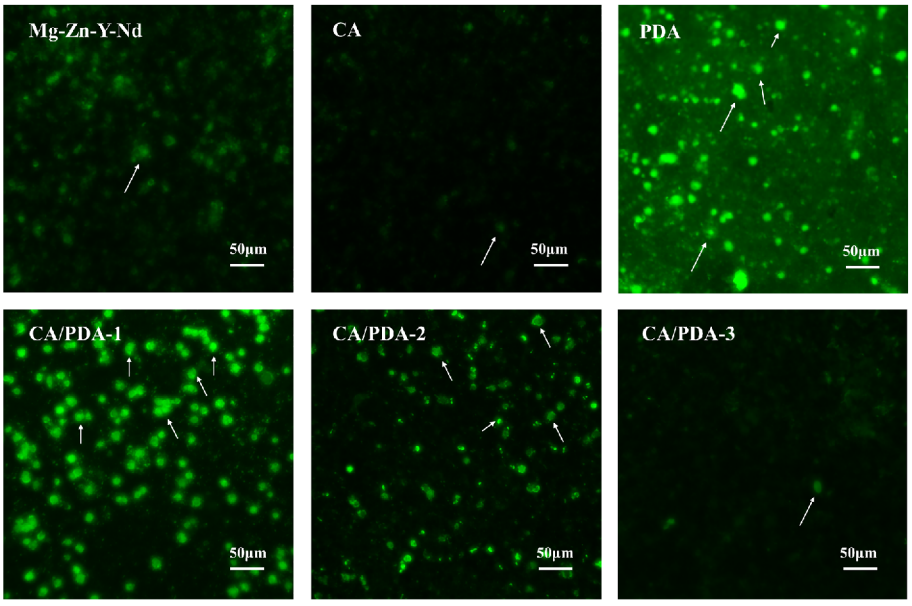

Figure 9 (Color online) Fluorescence images of HUVEC on samples of Mg-Zn-Y-Nd, CA, PDA, CA/PDA-1, CA/PDA-2 and CA/PDA-3, respectively. The spots pointed by arrows were the HUVEC that stained with rhodamine.

coverage ratio compared with CA/PDA-1 and CA surfaces. The CCK-8 determination and HUVEC coverage ratio calculation in Figure 10 showed the consistent results, and all the results indicated that the CA/PDA-1 layer could significantly improve the endothelialization of Mg-Zn-Y-Nd substrate.

3.4 Vascular smooth muscle cells growth

After the stent intervention, the smooth muscle cells that located at the blood vessel media will be triggered by the damaged vessel wall, then pathologically proliferated and migrated on to the stents' surfaces, which will lead to hyperplasia and make key challenge for the long-term therapy [43,44]. Thus, the HUASMC number on each surface was investigated to evaluate the anti-hyperplasia ability. The DAPI staining images (Figure 11) and CCK-8 determination (Figure 12) of HUASMC indicated that Mg-Zn-Y-Nd substrate presented a very low HUASMC number, while the CA and CA/PDA-1 modification further reduced HUASMC number, suggesting better anti-hyperplasia function. Contrarily, PDA deposition increased HUASMC number due to its amine group, and higher amine density may cause more HUASMC number, which was proved by the results from CA/PDA-2 and CA/PDA-3 surface. This results also validated the fact that distinct response from different cells (HUVEC, RBC and HUASMC, etc.) for the amine density change.

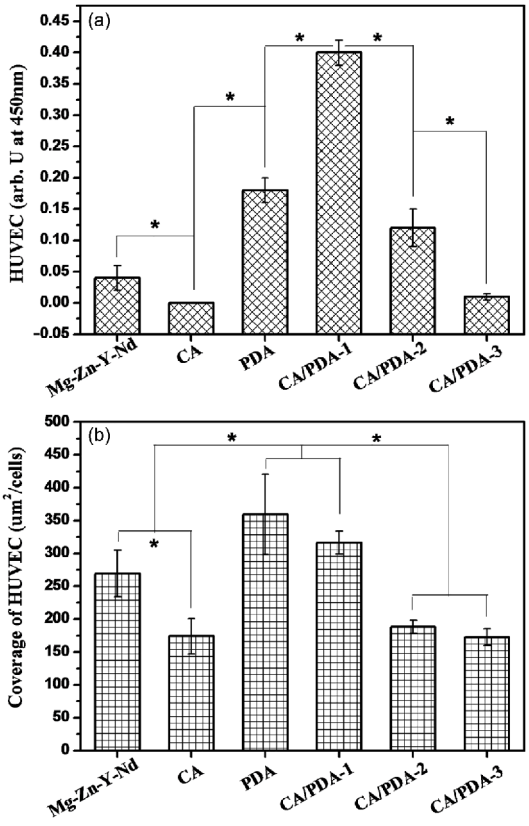

Figure 10 (a) Quantitative characterization and (b) coverage ratios of HUVEC on samples of Mg-Zn-Y-Nd, CA, PDA, CA/PDA-1, CA/PDA-2 and CA/PDA-3, respectively (mean±SD, *p<0.05, n=3).

3.5 Macrophages adhesion and activation

Inflammation is the first response of the immune system to infection, injury, or irritation, and macrophages play a crucial role during the inflammatory process [45]. The fluorescence photographs and counting of macrophages on the Mg-Zn-Y-

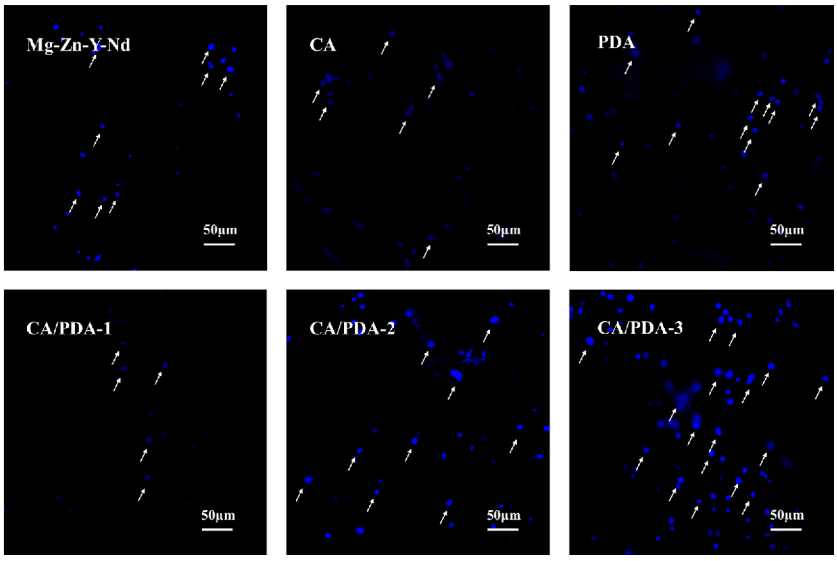

Figure 11 (Color online) Fluorescence images of HUASMCs stained with DAPI on samples of Mg-Zn-Y-Nd, CA, PDA, CA/PDA-1, CA/PDA-2 and CA/PDA-3, respectively. The dots pointed by arrows were the HUASMC nucleus that stained with DAPI.

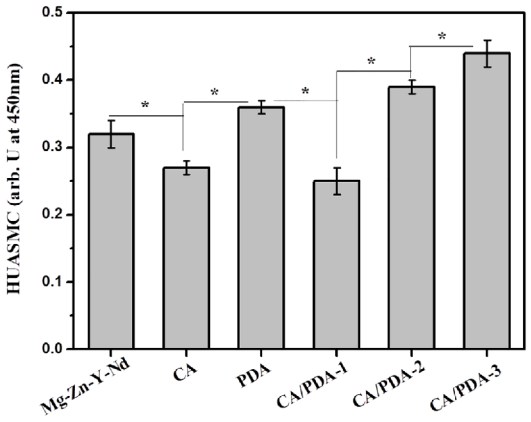

Figure 12 Quantitative characterization of HUASMCs on samples of Mg-Zn-Y-Nd, CA, PDA, CA/PDA-1, CA/PDA-2 and CA/PDA-3, respectively (mean±SD, $*p<0.05$, $n=3$).

Nd, CA, PDA, CA/PDA-1, CA/PDA-2 and CA/PDA-3 samples are shown in Figures 13 and 14(a). It could be seen from Figure 13 that very few macrophages distributed on the CA and CA/PDA-1 surfaces, and their nucleus presented rounded shape, which indicated a non-inflammation state, while numerous macrophages attached on the Mg-Zn-Y-Nd, PDA, CA/PDA-2 and CA/PDA-3 surfaces, and their nucleus possessed more area, suggesting the aggregated and/or activated state. The quantity of the attached macrophages on the surfaces presented in Figure 14(a) indicated that the CA and CA/PDA-1 samples showed significantly less macrophages compared with the other samples. It is very interesting that there is no significant difference between Mg-Zn-Y-Nd and PDA on macrophages numbers. This may be due to their different pro-inflammatory mechanisms: Mg-Zn-Y-Nd may lead to inflammation because of its excessive hydrogen enrichment during the degradation process [46], while the PDA preparation introduced amine group and further attracted more macrophages adhesion to the Mg-Zn-Y-Nd surface [24]. Another interesting phenomenon was that the attached macrophages numbers displayed a trend: CA/PDA-1<PDA<CA/PDA-2<CA/PDA-3. This trend was consistent with the amine group quantity and HUASMC quantity, but different from HUVEC and platelets quantity, which further verified the fact that distinct response from different cells (HUVEC, RBC, platelets, HUASMC and macrophages, etc.) for the amine density change.

During the inflammation reaction, the attached and activated macrophages on the devices will release special chemokines (such as TNF-α and IL-6), which may aggravate this pathological process [47]. Thus, TNF-α and IL-6 released from the macrophages on the Mg-Zn-Y-Nd, CA, PDA, CA/PDA-1, CA/PDA-2 and CA/PDA-3 samples were measured by a typical ELISA method, and the results are presented in Figure 14(b). It was obvious that macrophages on the CA and CA/PDA-1 layers released less TNF-α and IL-6 compared with the other samples, suggesting better anti-inflammation function.

4 Conclusions

In this work, the Mg-Zn-Y-Nd alloy substrate was modified with citric acid (CA) and dopamine by a layer-by-layer self-assembly method. The characterization of AFM, water contact angle measurement and carboxyl/amine quantity proved the successful preparation of the three CA/PDA layers (CA/PDA-1, CA/PDA-2 and CA/PDA-3). The dynamic blood test demonstrated the significantly improved blood compatibility of the Mg-Zn-Y-Nd by both CA and CA/

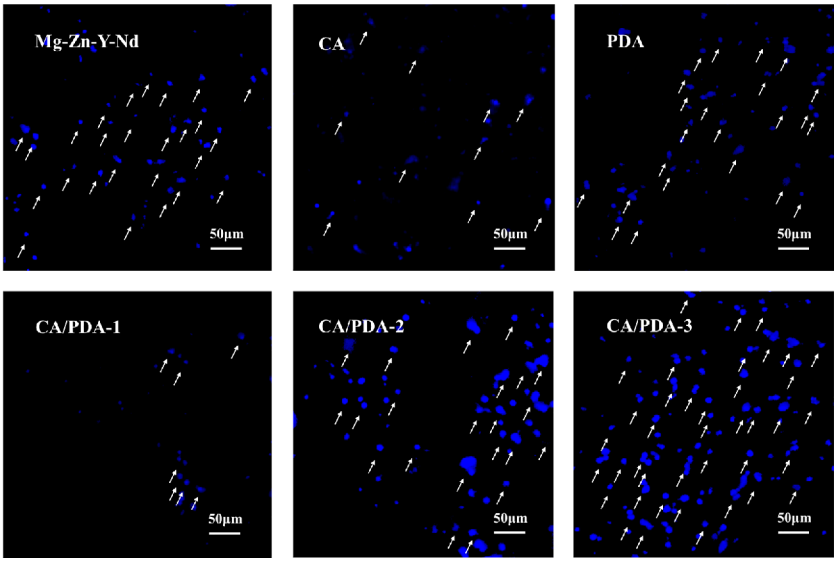

Figure 13 (Color online) Fluorescence images of macrophages stained with DAPI on samples of Mg-Zn-Y-Nd, CA, PDA, CA/PDA-1, CA/PDA-2 and CA/PDA-3, respectively. The dots pointed by arrows were the macrophage nucleus that stained with DAPI.

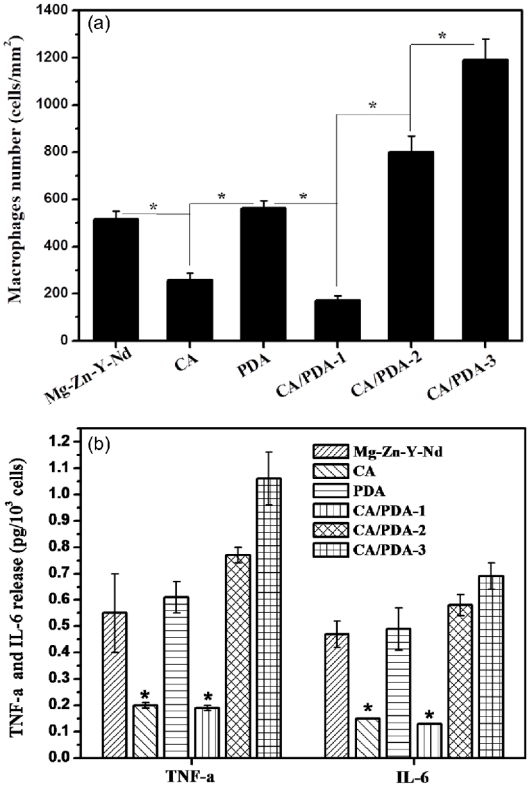

Figure 14 (a) Macrophages counting on samples of Mg-Zn-Y-Nd, CA, PDA, CA/PDA-1, CA/PDA-2 and CA/PDA-3, respectively (mean±SD, *p<0.05, n=3); (b) TNF-α and IL-6 release from macrophages on Mg-Zn-Y-Nd, CA, PDA, CA/PDA-1, CA/PDA-2 and CA/PDA-3, respectively (*p<0.05 compared with all the other samples, mean±SD, n=3).

PDA-1 modification, and the HUASMC culture experiment presented a consistent result that both the CA and CA/PDA-1 layers inhibited smooth muscle cell proliferation, suggesting a strong anti-hyperplasia function. In particular, the CA/PDA-1 layer exhibited excellent improving ability on endothelial cell growth and coverage, indicating potential function on pro-endothelialization. The macrophages culture results also showed that the CA/PDA-1 layer inhibited macrophages attachment and activated (TNF-α and IL-6 release), indicating better anti-inflammation functions. All the results revealed that this CA/PDA modification with specific parameters could markedly improve surface biocompatibility, especially promote endothelial cells growth, and thus was looked forward potentially application for surface modification of degradable magnesium alloy as cardiovascular implanted biomaterials.

This work was supported by the National Key Research and Development Program of China (Grant Nos. 2016YFC1102403 & 2017YFGX090043-04), Fostering Talents of National Natural Science Foundation of China and Henan Province (Grant No. U1504310), and National Center for International Research of Micro-nano Molding Technology & Key Laboratory for Micro Molding Technology of Henan Province (Grant No. MMT2017-01).

1 World Health Organization (WHO). Global status report on non-communicable diseases 2014. Geneva, 2014
2 Fuster V. Top 10 cardiovascular therapies and interventions for the next decade. Nat Rev Cardiol, 2014, 11: 671–683
3 Serruys P W, Kutryk M J B, Ong A T L. Coronary-artery stents. N Engl J Med, 2006, 354: 483–495
4 Ramcharitar S, Serruys P W. Fully biodegradable coronary stents. Am J Cardiovasc Drug, 2008, 8: 305–314
5 Moravej M, Mantovani D. Biodegradable metals for cardiovascular stent application: Interests and new opportunities. Int J Mol Sci, 2011, 12: 4250–4270
6 Yang H, Wang C, Liu C, et al. Evolution of the degradation mechanism of pure zinc stent in the one-year study of rabbit abdominal aorta model. Biomaterials, 2017, 145: 92–105
7 Erbel R, Di Mario C, Bartunek J, et al. Temporary scaffolding of coronary arteries with bioabsorbable magnesium stents: A prospective, non-randomised multicentre trial. Lancet, 2007, 369: 1869–1875

8 Liu J, Wang P, Chu C C, et al. Arginine-leucine based poly (ester urea urethane) coating for Mg-Zn-Y-Nd alloy in cardiovascular stent applications. Colloids Surf B, 2017, 159: 78–88
9 Liu J, Xi T. Enhanced anti-corrosion ability and biocompatibility of PLGA coatings on MgZnYNd alloy by BTSE-APTES pre-treatment for cardiovascular stent. J Mater Sci Tech, 2016, 32: 845–857
10 Wu Q, Zhu S, Wang L, et al. The microstructure and properties of cyclic extrusion compression treated Mg-Zn-Y-Nd alloy for vascular stent application. J Mech Behav Biomed Mater, 2012, 8: 1–7
11 Zhu S J, Liu Q, Qian Y F, et al. Effect of different processings on mechanical property and corrosion behavior in simulated body fluid of Mg-Zn-Y-Nd alloy for cardiovascular stent application. Front Mater Sci, 2014, 8: 256–263
12 Zhang K, Li J A, Deng K, et al. The endothelialization and hemocompatibility of the functional multilayer on titanium surface constructed with type IV collagen and heparin. Colloids Surf B, 2013, 108: 295–304
13 Li J, Zhang K, Chen H, et al. A novel coating of type IV collagen and hyaluronic acid on stent material-titanium for promoting smooth muscle cell contractile phenotype. Mater Sci Eng-C, 2014, 38: 235–243
14 Li J, Yang P, Zhang K, et al. Preparation of SiO_2/TiO_2 and TiO_2/TiO_2 micropattern and their effects on platelet adhesion and endothelial cell regulation. Nucl Instrum Methods Phys Res Sect B, 2013, 307: 575–579
15 Frattolin J, Barua R, Aydin H, et al. Development of a novel biodegradable metallic stent based on microgalvanic effect. Ann Biomed Eng, 2016, 44: 404–418
16 von Birgelen C, Kok M M, van der Heijden L C, et al. Very thin strut biodegradable polymer everolimus-eluting and sirolimus-eluting stents versus durable polymer zotarolimus-eluting stents in allcomers with coronary artery disease (BIO-RESORT): A three-arm, randomised, non-inferiority trial. Lancet, 2016, 388: 2607–2617
17 Cao F, Song G L, Atrens A. Corrosion and passivation of magnesium alloys. Corrosion Sci, 2016, 111: 835–845
18 Liu P, Pan X, Yang W, et al. Improved anticorrosion of magnesium alloy via layer-by-layer self-assembly technique combined with micro-arc oxidation. Mater Lett, 2012, 75: 118–121
19 Simonte F M, Dötsch A, Galego L, et al. Investigation on the anaerobic propionate degradation by *Escherichia coli* K12. Mol Microbiol, 2017, 103: 55–66
20 Ye M, Zhang L, Xu P, et al. Simultaneous analysis of ten low-molecular-mass organic acids in the tricarboxylic acid cycle and photorespiration pathway in *Thalassiosira pseudonana* at different growth stages. J Sep Sci, 2017, 40: 635–645
21 Martin M, Perez-Guaita D, Andrew D W, et al. The effect of common anticoagulants in detection and quantification of malaria parasitemia in human red blood cells by ATR-FTIR spectroscopy. Analyst, 2017, 142: 1192–1199
22 Lee H, Dellatore S M, Miller W M, et al. Mussel-inspired surface chemistry for multifunctional coatings. Science, 2007, 318: 426–430
23 Lee H, Lee B P, Messersmith P B. A reversible wet/dry adhesive inspired by mussels and geckos. Nature, 2007, 448: 338–341
24 Wu F, Li J, Zhang K, et al. Multifunctional coating based on hyaluronic acid and dopamine conjugate for potential application on surface modification of cardiovascular implanted devices. ACS Appl Mater Interfaces, 2016, 8: 109–121
25 Li J A, Zhang K, Xu Y, et al. A novel co-culture models of human vascular endothelial cells and smooth muscle cells by hyaluronic acid micro-pattern on titanium surface. J Biomed Mater Res A, 2014, 102A: 1950–1960
26 Li J, Li G, Zhang K, et al. Co-culture of vascular endothelial cells and smooth muscle cells by hyaluronic acid micro-pattern on titanium surface. Appl Surf Sci, 2013, 273: 24–31
27 Li J, Wu F, Zhang K, et al. Controlling molecular weight of hyaluronic acid conjugated on amine-rich surface: Toward better multifunctional biomaterials for cardiovascular implants. ACS Appl Mater Interfaces, 2017, 9: 30343–30358
28 Zhang K, Bai Y, Wang X, et al. Surface modification of esophageal stent materials by a polyethylenimine layer aiming at anti-cancer function. J Mater Sci-Mater Med, 2017, 28: 125
29 Kokubo T, Takadama H. How useful is SBF in predicting *in vivo* bone bioactivity? Biomaterials, 2006, 27: 2907–2915
30 Feng Y, Zhu S, Wang L, et al. Characterization and corrosion property of nano-rod-like HA on fluoride coating supported on Mg-Zn-Ca alloy. Bioact Mater, 2017, 2: 63–70
31 Li J, Zhang K, Yang P, et al. Human vascular endothelial cell morphology and functional cytokine secretion influenced by different size of HA micro-pattern on titanium substrate. Colloids Surfs B-Biointerfaces, 2013, 110: 199–207
32 Xiang L, Li J, He Z, et al. Design and construction of TiO_2 nanotubes in microarray using two-step anodic oxidation for application of cardiovascular implanted devices. Micro Nano Lett, 2015, 10: 287–291
33 Wu J, Li J, Wu F, et al. Effect of micropatterned TiO_2 nanotubes thin film on the deposition of endothelial extracellular matrix: For the purpose of enhancing surface biocompatibility. Biointerphases, 2015, 10: 04A302
34 Li J, Zhang K, Wu J, et al. Co-culture of endothelial cells and patterned smooth muscle cells on titanium: Construction with high density of endothelial cells and low density of smooth muscle cells. Biochem Biophys Res Commun, 2015, 456: 555–561
35 Li J, Zhang K, Yang P, et al. Research of smooth muscle cells response to fluid flow shear stress by hyaluronic acid micro-pattern on a titanium surface. Exp Cell Res, 2013, 319: 2663–2672
36 Li L, Xu Y, Zhou Z, et al. The effects of Cu-doped TiO_2 thin films on hyperplasia, inflammation and bacteria infection. Appl Sci, 2015, 5: 1016–1032
37 Li J, Zhang K, Wu J, et al. Tailoring of the titanium surface by preparing cardiovascular endothelial extracellular matrix layer on the hyaluronic acid micro-pattern for improving biocompatibility. Colloids Surf B, 2015, 128: 201–210
38 Zhou Z, Chen J, Xiang L, et al. Fabrication of 3D TiO_2 micromesh on silicon surface and its effects on platelet adhesion. Mater Lett, 2014, 132: 149–152
39 Li J, Zou D, Zhang K, et al. Strong multi-functions based on conjugating chondroitin sulfate onto an amine-rich surface will direct the vascular cell fate for cardiovascular implanted devices. J Mater Chem B, 2017, 5: 8299–8313
40 Manakhov A, Kedroňová E, Medalová J, et al. Carboxyl-anhydride and amine plasma coating of PCL nanofibers to improve their bioactivity. Mater Des, 2017, 132: 257–265
41 Zhang E, Shen F. Blood compatibility of a ferulic acid (FA)-eluting PHBHHx system for biodegradable magnesium stent application. Mater Sci Eng-C, 2015, 52: 37–45
42 Liu X, Zhen Z, Liu J, et al. Multifunctional MgF_2/polydopamine coating on mg alloy for vascular stent application. J Mater Sci Tech, 2015, 31: 733–743
43 Wang F, Li C, Ding F H, et al. Increased serum TREM-1 level is associated with in-stent restenosis, and activation of TREM-1 promotes inflammation, proliferation and migration in vascular smooth muscle cells. Atherosclerosis, 2017, 267: 10–18
44 Kim J H, Bae K H, Byun J K, et al. Lactate dehydrogenase-A is indispensable for vascular smooth muscle cell proliferation and migration. Biochem Biophys Res Commun, 2017, 492: 41–47
45 Wen H, Liu M, Liu Z, et al. PEDF improves atherosclerotic plaque stability by inhibiting macrophage inflammation response. Int J Cardiol, 2017, 235: 37–41
46 Liu J, Zheng B, Wang P, et al. Enhanced *in vitro* and *in vivo* performance of Mg-Zn-Y-Nd alloy achieved with APTES pretreatment for drug-eluting vascular stent application. ACS Appl Mater Interfaces, 2016, 8: 17842–17858
47 Singh P, Kaur S, Sharma A, et al. TNF-α and IL-6 inhibitors: Conjugates of N-substituted indole and aminophenylmorpholin-3-one as anti-inflammatory agents. Eur J Med Chem, 2017, 140: 92–103